

# Prevalence of Venovenous Shunting and High-Output State Quantified with 4D Flow MRI in Patients with Fontan Circulation

Francesca Raimondi, MD • Duarte Martins, MD • Raluca Coenen, MD • Elena Panaioli, MD • Diala Khraiche, MD • Nathalie Boddaert, MD, PhD • Damien Bonnet, MD, PhD • Melany Atkins, MD • Howaida El-Said, MD, PhD • Laith Alshawabkeh, MD • Albert Hsiao, MD, PhD

From the Unité Médico-Chirurgicale de Cardiologie Congénitale et Pédiatrique, Centre de Référence des Maladies Cardiaques Congénitales Complexes-M3C, Hôpital Universitaire Necker-Enfants Malades, Université de Paris, Paris, France (F.R., D.K., D.B.); Pediatric Radiology Unit, Hôpital Universitaire Necker-Enfants Malades, Université de Paris, Paris, France (F.R., E.P., N.B.); Decision and Bayesian Computation, Computation Biology Department, CNRS, URS 3756, Neuroscience Department, CNRS UMR 3571, Institut Pasteur, Paris, France (F.R.); School of Biomedical Engineering & Imaging Sciences, King's College London, Lambeth Wing, St Thomas' Hospital, London, England (F.R.); Department of Pediatric Cardiology, Hospital de Santa Cruz, Centro Hospitalar Lisboa Ocidental, Lisbon, Portugal (D.M.); Radiology and Cardiology Unit, Erasmus MC, Rotterdam, the Netherlands (R.C.); Fairfax Radiological Consultants, Fairfax, Va (M.A.); and Departments of Pediatric Cardiology (H.E.S.), Cardiovascular Medicine (L.A.), and Radiology (A.H.), University of California, San Diego, 9300 Campus Point Dr, Room 7756, La Jolla, CA 92037-7756. Received June 3, 2021; revision requested July 27; revision received November 4; accepted November 12. Address correspondence to A.H. (e-mail: Hsiao@ucsd.edu).

Authors declared no funding for this work.

Conflicts of interest are listed at the end of this article.

Radiology: Cardiothoracic Imaging 2021; 3(6):e210161 • <https://doi.org/10.1148/ryct.210161> • Content codes:  

**Purpose:** To assess the ability of four-dimensional (4D) flow MRI to quantify flow volume of the Fontan circuit, including the frequency and hemodynamic contribution of systemic-to-pulmonary venovenous collateral vessels.

**Materials and Methods:** In this retrospective study, patients with Fontan circulation were included from three institutions (2017–2021). Flow measurements were performed at several locations along the circuit by two readers, and collateral shunt volumes were quantified. The frequency of venovenous collaterals and structural defects were tabulated from concurrent MR angiography, contemporaneous CT, or catheter angiography and related to Fontan clinical status. Statistical analysis included Pearson and Spearman correlation and Bland-Altman analysis.

**Results:** Seventy-five patients (mean age, 20 years; range, 5–58 years; 46 female and 29 male patients) were included. Interobserver agreement was high for aortic output, pulmonary arteries, pulmonary veins, superior vena cava (Glenn shunt), and inferior vena cava (Fontan conduit) (range,  $\rho = 0.913$ – $0.975$ ). Calculated shunt volume also showed strong agreement, on the basis of the difference between aortic and pulmonary flow ( $\rho = 0.935$ ). A total of 37 of 75 (49%) of the patients exhibited shunts exceeding 1.00 L/min, 81% (30 of 37) of whom had pulmonary venous or atrial flow volume step-ups and corresponding venovenous collaterals. A total of 12% of patients (nine of 75) exhibited a high-output state ( $>4$  L/min/m<sup>2</sup>), most of whom had venovenous shunts exceeding 30% of cardiac output.

**Conclusion:** Fontan flow and venovenous shunting can be reliably quantified at 4D flow MRI; high-output states were found in a higher proportion of patients than expected, among whom venovenous collaterals were common and constituted a substantial proportion of cardiac output.

Supplemental material is available for this article.

© RSNA, 2021

Post-Fontan procedure single-ventricle physiology is among the most complex congenital heart diseases to manage, as it is associated with high morbidity and mortality (1). The Fontan procedure was originally conceived in 1971 for palliation of tricuspid atresia (2); since then, the procedure has undergone several technical revisions and is now a common endpoint for single-ventricle pathologic conditions. While the majority ( $>90\%$ ) of patients with Fontan circulation now survive to adult age (3), the Fontan palliation has several known long-term complications, including ventricular failure, hepatic cirrhosis, and lymphatic complications such as protein-losing enteropathy and plastic bronchitis. Thromboembolism and thrombosis of the Fontan circuit can also contribute to Fontan failure. Therefore, attentive surveillance during follow-up is crucial for the

clinical management of patients who have undergone the Fontan procedure (4).

Noninvasive cardiac imaging provides essential information about the anatomic and physiologic status of the Fontan circulation, which has been used to better manage and mitigate potential complications (5). Traditionally, this has included evaluation of atrial septal anatomy, ventricular function, atrioventricular and systemic valve function, anatomy of Fontan conduit, collateral flow, aortic arch anatomy, fenestration flow, and myocardial fibrosis (6,7). Echocardiography remains a first-line modality for initial evaluation, capable of evaluating multiple aspects of the Fontan circuit and ventricle (8). However, several aspects of the complex anatomy of the Fontan circuit are obscured from echocardiographic interrogation and benefit from MRI

## Abbreviations

4D = four dimensional, IVC = inferior vena cava, kat-ARC = k-adaptive-t autocalibrating,  $Q_{Ao-Cavac}$  = shunt flow relative to cavea,  $Q_{Ao-PA}$  = shunt flow relative to pulmonary arteries, SVC = superior vena cava,  $v_{enc}$  = velocity encoding

## Summary

In a large multi-institutional study, four-dimensional flow MRI provided highly reliable clinical quantification of flow volume for management of patients with a Fontan circuit and revealed an unexpectedly high frequency of venovenous shunting, contributing to high-output failure.

## Key Points

- Venous and arterial flow measurements can be readily performed along the Fontan circuit with four-dimensional flow MRI with high interobserver consistency (range of  $\rho = 0.913$ – $0.975$  across seven measurements).
- Systemic-to-pulmonary venous shunts are common in patients with Fontan palliation, with 32% (24 of 75) of patients exhibiting a pulmonary venous or atrial “step-up” exceeding 1.00 L/min, excluding patients with fenestrations or aortopulmonary collateral vessels.
- Though Fontan circulation is generally considered a low-output state, 12% (nine of 75) of patients exhibited high-output state, and most of these patients had large venovenous collateral vessels as the underlying cause.

## Keywords

Pediatrics, MR Angiography, Cardiac, Technology Assessment, Hemodynamics/Flow Dynamics, Congenital

evaluation, including the assessment of myocardial scar and quantification of systemic-to-pulmonary collateral venous flow (9).

Most recently, four-dimensional (4D) flow MRI has emerged as a promising technique to gain hemodynamic insights in patients with a Fontan circuit (10,11). Recent studies have begun to show that 4D flow may be more reliable than conventional phase-contrast MRI for the quantification of blood flow volume (12–15) and ability to quantify inlet valvular regurgitation (16,17). Additionally, there is a closer relationship to shunt fraction measurements from 4D flow MRI compared with those obtained during cardiac catheterization (18). At present, however, there is a paucity of large-scale 4D flow MRI studies in the clinical environment, and its efficacy for detecting clinically relevant hemodynamic abnormalities in patients with a Fontan circuit remains to be determined. Particular to the Fontan circulation, which is typically considered a chronic state of low-output heart failure, it is unknown with what frequency venovenous collateral vessels are present and impact Fontan physiology, beyond the observation that they are a treatable cause of cyanosis (4).

Therefore, we sought to retrospectively examine the effectiveness of 4D flow MRI in evaluating patients with a Fontan circuit by aggregating our experience at three institutions that have incorporated this technology into clinical routine. We sought specifically to: (a) assess the relative reliability of flow volume measurements at multiple points along the Fontan circuit and (b) observe the frequency of venous shunting with 4D flow MRI.

## Materials and Methods

### Patient Sample

We retrospectively included all patients with a history of Fontan palliation who were referred to three tertiary hospitals for cardiac MRI including a 4D flow acquisition. The study respected European General Data Protection Regulation law on retrospective studies (MR004 conformity) for site A. For sites in the United States, studies were performed with Health Insurance Portability and Accountability Act compliance and in compliance with local institutional review board–approved research studies, including waiver of informed consent for site B and written informed consent for site C.

A total of 89 MRI examinations were identified: 32 examinations from site A, 46 examinations from site B, and 11 examinations from site C. Examinations with nondiagnostic MRI were excluded from the study, exclusively due to signal dephasing artifact from metallic coils from prior venovenous collateral embolization precluding visualization and flow measurement in more than one vessel (one from site A, 10 from site B, and two from site C). One patient from site C underwent two MRI examinations during the study period, and only the latter was included in the analysis. A total of 75 patients were included in the study.

### Acquisition 4D Flow Image Data

4D flow MRI acquisitions were performed using retrospective electrocardiographic gating during free breathing without the use of respiratory gating. All acquisitions covered the entire chest, including the heart and Fontan circulation in an axial volume. Each site selected their imaging technique, including velocity-encoding ( $v_{enc}$ ) speed, on the basis of local preferences. Temporal resolution was estimated on the basis of temporal sampling ( $4\times$  repetition time) instead of number of reconstructed image phases.

For site A, MRI examinations in 32 patients were included, from May 2017 through March 2021. 4D flow was performed with a 1.5-T Discovery MR450 (GE Healthcare) following administration of gadolinium-based contrast agent gadobutrol (Gadovist 1 mmol/mL; Bayer). 4D flow MRI was performed with a k-adaptive-t autocalibrating (kat-ARC)–accelerated cartesian 4D flow MRI sequence (GE Healthcare). The parameters for site A were as follows: repetition time, 2.7 msec; echo time, 2.2 msec; flip angle,  $14^\circ$ ; acquisition voxel,  $1.7 \times 2.0 \times 2.0$  mm. Temporal resolution was automatically tailored to heart rate (range, 17–69 msec; mean, 46 msec). The  $v_{enc}$  value was individually adapted to yield images without aliasing artifacts, on the basis of prior echocardiographic peak velocity (200–550 cm/sec). Acquisition time ranged from 7 minutes 30 seconds to 13 minutes 43 seconds (mean, 10 minutes 26 seconds).

For site B, MRI examinations in 36 patients were included, from February 2017 through March 2021. 4D flow acquisitions were performed immediately following a contrast-enhanced MR angiography performed with administration of 0.15 mmol of gadobenate dimeglumine (Multihance; Bracco Imaging) per kilogram of body weight. Imaging was performed with a 3-T Discovery MR750 with a 32-channel phased-array

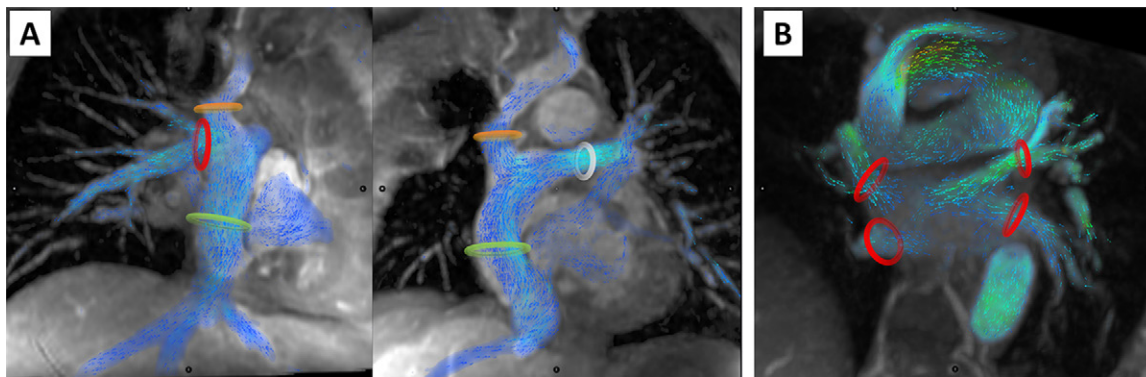


**Figure 1:** Measurement of systemic and pulmonary venous return in the Fontan circuit. In **(A)**, the superior vena cava, or Glenn shunt (orange ring), the inferior vena cava, or Fontan conduit (green ring), right pulmonary artery (red ring), and left pulmonary artery (white ring) indicate the locations of flow volume measurement of passive systemic venous return. In **(B)**, the red rings mark the locations of flow volume measurement of each of the pulmonary veins.

coil (GE Healthcare). 4D flow MRI was performed using a noncommercial pulse sequence with a three-dimensional cartesian strategy (ky-kz) in which samples were grouped in spiral-like sets and acquired with golden angle ordering (19,20), evenly spaced over time with dense central k-space sampling for respiratory soft gating (21). Mean parameters for site B were as follows: repetition time, 5.03 msec; echo time, 2.65 msec; flip angle, 25°; acquisition resolution,  $1.90 \times 2.28 \times 2.90$  mm. Temporal resolution was automatically tailored to heart rate (range, 27–81 msec; mean, 48 msec). A  $v_{enc}$  speed of 120–250 cm/sec was selected (mean, 155 cm/sec). Acquisition time ranged from 10 minutes 13 seconds to 15 minutes 25 seconds (mean, 12 minutes 23 seconds).

For site C, MRI examinations in eight patients were included, from April 2017 through October 2020. 4D flow acquisitions were performed after administration of 90 mg of ferumoxytol (Feraheme; AMAG Pharmaceuticals) per kilogram of body weight, diluted with saline in a 1:4 ratio, injected at 2 mL/sec. Imaging was performed with either a 1.5-T Discovery MR450 or a 3-T Discovery MR750 (GE Healthcare) with a phased-array receiver coil. 4D flow MRI was performed with a kat-ARC-accelerated cartesian 4D flow MRI sequence (GE Healthcare). Mean parameters for site C were as follows: repetition time, 4.57 msec; echo time, 2.44 msec; flip angle, 15°; acquisition resolution,  $1.96 \times 1.96 \times 2.60$  mm. A  $v_{enc}$  speed of 250–300 cm/sec was selected. Temporal resolution was automatically tailored to heart rate (range, 41–75 msec; mean, 62 msec). Acquisition time ranged from 5 minutes 26 seconds to 12 minutes 10 seconds (mean, 7 minutes 56 seconds).

### Analysis of 4D Flow Image Data

All 4D flow image data were processed using Arterys version 25.5.1, a cloud-based platform used to share images across sites and perform postprocessing analysis, which includes performing background phase-error correction, as well as visualization with 4D multiplanar image reconstruction and quantification of blood flow. Measurements were performed independently by two subspecialty cardiovascular radiologists (F.R. and A.H.), each with more than 10 years of experience in cardiac imaging and 4 years and more than 10 years of experience, respectively,

specifically with 4D flow. Each reader was blinded to measurements from the other reader and were also blinded from any clinical background information.

Flow measurements were performed at several locations along the Fontan circuit (Fig 1). Measurements of the Fontan flow were performed where flow was most laminar, at the inferior vena cava (IVC) junction for patients with dilated atrial conduits, or within the conduit itself for extracardiac or lateral tunnel Fontan. IVC flow measurement was performed above fenestrations, when possible, but this was sometimes precluded by complex geometry. Measurements of the superior vena cava (SVC) or Glenn shunt, right pulmonary artery, left pulmonary artery, right pulmonary veins, left pulmonary veins, and aortic output were also performed. Pulmonary veins were individually segmented and summed to provide total pulmonary venous flow for each side. Similarly, if a single measurement was not possible for the main pulmonary arteries, individual branch pulmonary arteries were segmented and summed. Aortic output was measured in the ascending aorta or systemic valve(s). For Damus-Kaye-Stansel repairs, the two outlet valves were segmented and summed if the ascending aortic flow was not laminar or obscured by metallic artifact.

### Ventricular Volumetry and Function

At each site, cine steady-state free precession imaging was performed with a short-axis stack for cardiac volumetry and function. Images were analyzed according to standard of clinical practice at each institution with their preferred clinical analysis software. Volumetric measurements were tabulated for each patient where available, excluding one patient for whom cine steady-state free precession imaging was aborted due to claustrophobia. Cardiac volumes were normalized by body surface area (Dubois-Dubois).

### Shunt Volume Quantification

For each side, collateral shunt volume to the pulmonary veins was estimated as the difference between pulmonary venous return and pulmonary arterial flow. Collateral shunt volume to the atrium was estimated as the difference between aortic output and sum of pulmonary veins. Additionally, total shunt

volume was estimated according to two methods, either (a)  $Q_{Ao-Cavac}$ , computed as the difference between aortic output and the sum of the Glenn and Fontan flow, or (b)  $Q_{Ao-PA}$ , computed as the difference between aortic output and sum of right and left pulmonary arterial flow.

Total shunt volumes exceeding 1.0 L/min by either method were considered substantial shunts, and concurrent 4D flow and MR angiographic images were further analyzed to delineate the sources of shunting. All sources of collateral blood flow were tabulated, including aortopulmonary arterial collaterals, venous collaterals, and Fontan fenestrations, by consensus of two readers. Shunt volumes exceeding 750 mL/min to each target vessel (pulmonary veins or atrium) were considered substantial. Additionally, for all patients who underwent catheter angiography or CT angiography within 12 months, the presence or absence of aortopulmonary collaterals, Fontan fenestrations, and venovenous collaterals were tabulated. Venovenous collaterals were defined as dilated veins arising from systemic veins, observed to drain into pulmonary arteries, pulmonary veins, or atrium.

**Statistical Analysis**

Pearson correlation, Spearman correlation, and Bland-Altman analysis were used to assess interobserver consistency of flow measurements at each level of the Fontan circulation. Statistical analyses were performed with GraphPad Prism.

**Results**

**Patient Demographic and Clinical Characteristics**

Demographic characteristics of the 75 included patients are summarized in Table 1. A total of 34 patients were pediatric and 42 were adults, with ages ranging from 5 to 58 years (mean, 20 years). Forty-six patients were male and 29 were female. Patient age at Fontan completion ranged from 5 months to 30 years. The most common morphologic entity in this population was tricuspid atresia (25 of 75, 33%), followed by hypoplastic left heart (18 of 75, 24%), pulmonary atresia with intact ventricular septum (six of 75, 8%), atrioventricular canal (10 of 75, 13%), and double-inlet left ventricle (eight of 75, 11%). Among these patients, several patients had failing Fontan, requiring surgery, listing for cardiac transplantation, or were undergoing cardiac transplantation during the study period (nine of 75, 12%).

**Interreader Consistency of Blood Flow Measurements**

Blood flow volume measurements at each of the locations along the Fontan circuit showed high interreader consistency (Table 2). Measurements showed high agreement for all measurement locations, particularly the SVC or Glenn shunt ( $\rho = 0.973$ ), IVC or Fontan circuit ( $\rho = 0.947$ ), right pulmonary arteries ( $\rho = 0.975$ ), left pulmonary arteries ( $\rho = 0.954$ ), and aortic output ( $\rho = 0.964$ ). Measurements of the right pulmonary veins ( $\rho = 0.927$ ) and left pulmonary veins ( $\rho = 0.913$ ) also showed high, but slightly lower, agreement. This yielded similar relationships in the interobserver correlation of computed measurements of pulmonary flow distribution and collateral flow. Pulmonary

**Table 1: Summary of Patient Demographics and Clinical Characteristics**

Characteristic	Value
Sex	46 male, 29 female
Age at MRI (y)	20 (5–58)
Age at Fontan completion (y)	4 (1–19)
BSA (m <sup>2</sup> )	1.6 (0.68–2.26)
Aortic output (L/min)	4.79 (2.66–8.03)
Cardiac index (L/min/m <sup>2</sup> )	3.1 (1.82–5.82)
Structure	
Tricuspid atresia	25
Hypoplastic left heart	18
Atrioventricular canal	10
Double-outlet right ventricle	4
Double-inlet left ventricle	8
Pulmonary atresia with intact ventricular septum	6
Other	4
Fontan connection	
Extracardiac conduit	47
Lateral tunnel	15
Atriopulmonary connection	13
Institution	
Site A	31
Site B	36
Site C	8

Note.—Continuous variables are shown as mean with range in parentheses; all other values are numbers. BSA = body surface area.

venous flow distribution ( $\rho = 0.916$ ) and pulmonary arterial flow distribution ( $\rho = 0.951$ ) both showed high interobserver consistency. Estimates of collateral flow showed greater interobserver consistency by  $Q_{Ao-PA}$  ( $\rho = 0.934$ ) than  $Q_{Ao-Cavac}$  ( $\rho = 0.864$ ).

**Cardiac Output and Volumetry**

Based on 4D flow measurements of aortic flow volume, systemic cardiac output ranged from 2.66 to 8.03 L/min (median, 4.52 L/min), and cardiac index ranged from 1.82 to 5.82 L/min/m<sup>2</sup> (median, 2.89 L/min/m<sup>2</sup>). A total of 19% (14 of 75) of patients exhibited low output (cardiac index < 2.5 L/min/m<sup>2</sup>), and 12% (nine of 75) of patients exhibited high output (cardiac index > 4.0 L/min/m<sup>2</sup>). There was no correlation of cardiac output to ejection fraction. Stroke volume varied widely in this population, ranging from 27 to 131 mL/m<sup>2</sup> (median, 42 mL/m<sup>2</sup>).

**Visualization of Fontan Flow and Shunts**

Examples highlighting the visualization of shunts at 4D flow MRI in several patients are shown in Figures 2–4. With streamline rendering, we found it possible to trace the distribution of inferior (Fontan) and superior (Glenn) caval flow (Fig 5). Vi-

**Table 2: Interreader Consistency of Flow Volume Measurements and Computed Shunt Volumes along the Fontan Circuit**

Measurement	Spearman $r$	Pearson $\rho$	Bland-Altman
Glenn	0.953	0.973	0.021 (−0.303, 0.346)
Fontan	0.934	0.947	0.095 (−0.538, 0.728)
RPA	0.962	0.975	0.100 (−0.250, 0.450)
LPA	0.942	0.954	0.105 (−0.277, 0.487)
RPV	0.901	0.927	−0.195 (−0.348, 0.775)
LPV	0.911	0.913	0.077 (−0.396, 0.550)
Aorta	0.949	0.964	0.100 (−0.449, 0.649)
$Q_{Ao-Cavae}$	0.873	0.864	−0.015 (−0.859, 0.830)
$Q_{Ao-PA}$	0.918	0.934	−0.098 (−0.747, 0.551)
$Q_{RPV-RPA}$	0.745	0.848	0.095 (−0.588, 0.778)
$Q_{LPV-LPA}$	0.740	0.813	−0.026 (−0.583, 0.532)
$Q_{Ao-PV}$	0.719	0.789	−0.172 (−0.990, 0.646)

Note.—Bland-Altman mean differences and 95% limits of agreement (in parentheses) are provided in liters per minute. LPA = left pulmonary artery, LPV = left pulmonary veins,  $Q_{Ao-Cavae}$  = shunt flow relative to cavae,  $Q_{Ao-PA}$  = shunt flow relative to pulmonary arteries,  $Q_{Ao-PV}$  = shunt flow relative to pulmonary veins,  $Q_{LPV-LPA}$  = shunt flow to left pulmonary veins,  $Q_{RPV-RPA}$  = shunt flow to right pulmonary veins, RPA = right pulmonary artery, RPV = right pulmonary veins.

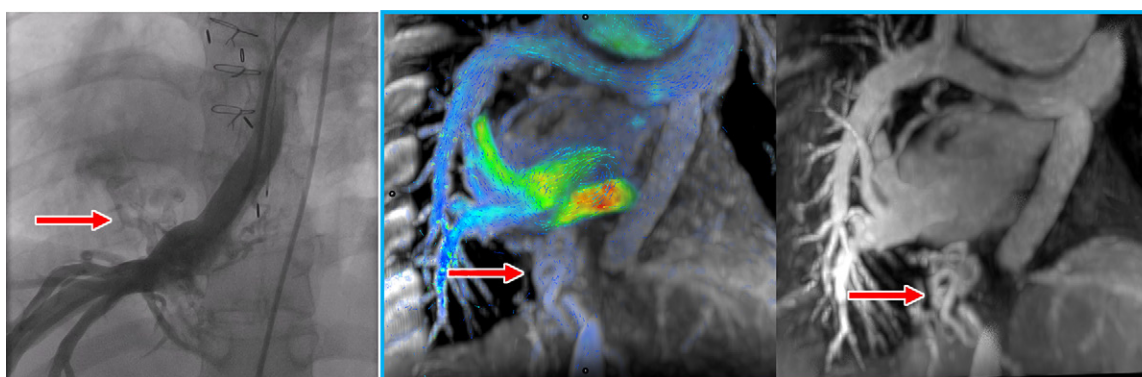


**Figure 2:** Venovenous collateral vessels (red arrows) at (from left to right) catheter angiography, four-dimensional (4D) flow, and contrast-enhanced MR angiography in a 27-year-old man with pulmonary atresia. These collateral vessels arise from the hepatic veins and directly drain into right pulmonary veins, bypassing the Fontan and pulmonary arteries to the lower-pressure pulmonary veins. Contrast-enhanced MR angiography can be performed in a single breath hold immediately preceding the free-breathing 4D flow scan in the same session as part of a comprehensive congenital heart MRI and MR angiography.

sualization of each of the structures of the Fontan circuit was noticeably clearer with smoother flow volume waveforms at acquisitions performed with lower  $v_{enc}$  speed, as expected. Among the few patients who underwent transthoracic echocardiography with interrogation of pulmonary veins, we observed that pulmonary venous flow waveforms of low  $v_{enc}$  acquisitions were morphologically similar to those observed echocardiographically (Fig 6; Movies 1, 2).

#### Frequency of Fontan Collaterals and High-Output State

Half (37 of 75, 49%) of all patients with Fontan circulation in our study exhibited substantial shunts exceeding a total volume greater than 1.0 L/min. A third of these patients (13 of 75, 17%) had shunts exceeding 30% of the cardiac output. Among

patients with substantial shunts, a small minority exhibited aortopulmonary collaterals (five of 37, 14%), few had fenestrations (eight of 37, 22%), while most had venovenous collaterals (30 of 37, 81%). Among patients who had visible venovenous collaterals, most caused a greater than 750 mL/min step-up in flow volume in the right pulmonary veins (18 of 30, 49%), while fewer caused a step-up in flow volume to the left pulmonary veins (six of 30, 16%). Excluding patients who had Fontan fenestrations, we also observed that many patients with venovenous collaterals exhibited a step-up of flow volume in the atrium (10 of 26, 38%). Among patients with substantial shunts, 58% (21 of 37) underwent CT angiography or catheter angiography within 1 year. Of these, all patients with substantial venovenous collaterals at 4D flow MRI were confirmed to

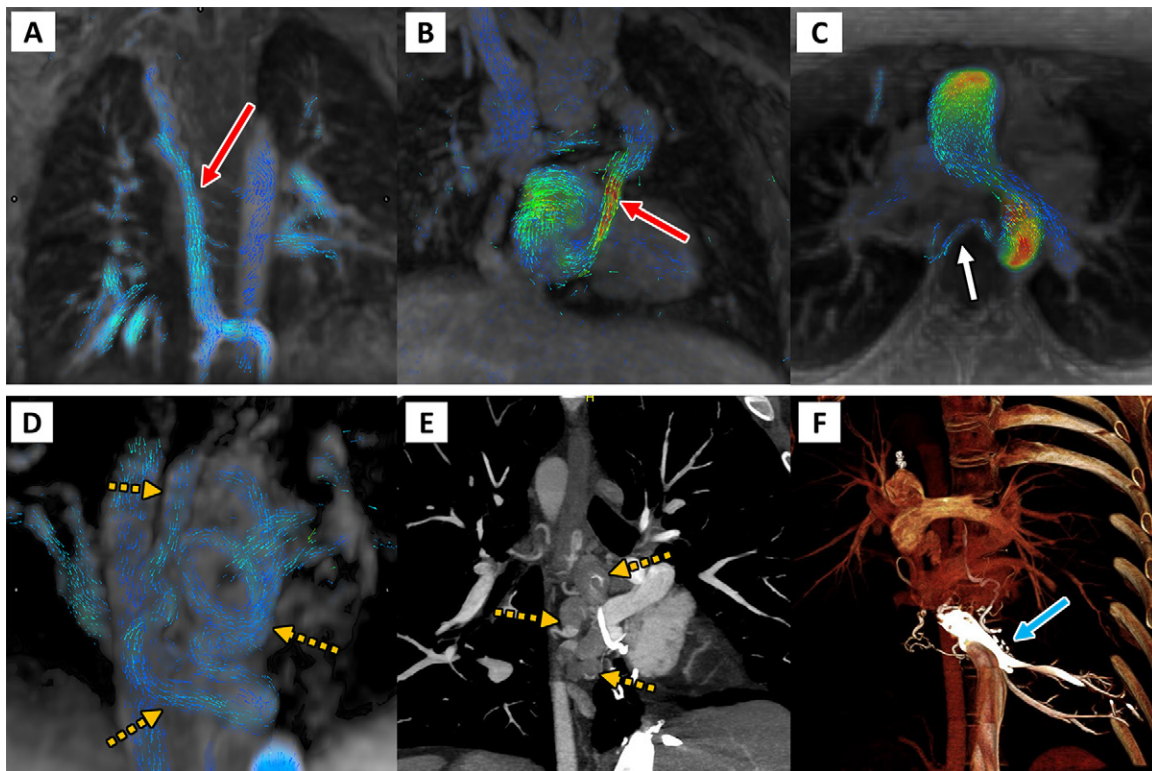


**Figure 3:** Four-dimensional (4D) flow visualization of venovenous and aortopulmonary collateral vessels to determine the cause of systemic-pulmonary venous shunting. First are two patients with large venovenous collateral vessels (red arrow), **(A)** a 5-year-old boy and **(B)** a 12-year-old boy, with drainage directly into the atrium bypassing the pulmonary arteries. **(C)** In a 13-year-old girl, a small aortopulmonary collateral artery is seen arising from the descending thoracic aorta (white arrow). Finally, on the bottom row, a 33-year-old man with large serpiginous venous collateral vessels (orange dashed arrows in **D** and **E**) is shown on **(D)** 4D flow and on **(E, F)** cardiac CT angiographic images, illustrating large venous varices and their direct supply from the hepatic venous confluence (blue arrow).

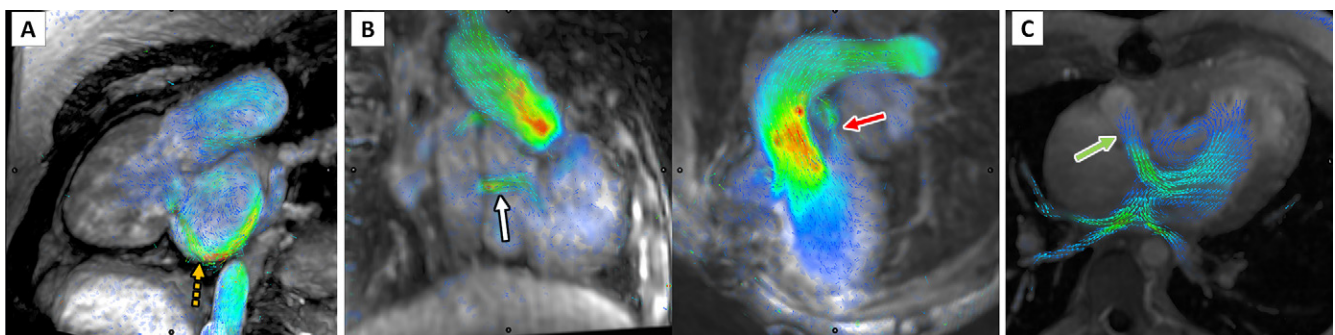


**Figure 4:** Four-dimensional flow visualization of atrioventricular valve insufficiency and additional shunts. **(A)** Image in a 24-year-old man with atrioventricular canal with severe inlet valve regurgitation during late systole, indicated by the orange dashed arrow. Note the absence of aortic flow as the ventricular pressure decompresses into the atrium. **(B)** Images in a 6-year-old girl with double-outlet right ventricle with Fontan fenestration (white arrow) and incomplete ligation of the pulmonary artery (red arrow). **(C)** Image in a 28-year-old man with right-to-left flow through a fenestration (green arrow) from an atrial Fontan.

have venovenous collaterals arising from systemic veins at CT or catheter angiography (Figs E1, E2 [supplement]).

Among patients with high cardiac output in excess of 4.0 L/min/m<sup>2</sup>, all had shunt volumes exceeding 1.0 L/min, suggesting shunting as a driving factor of the high-output state. In this group, the average shunt volume was 1.84–2.09 L/min depending on method used. Shunt volumes estimated using the  $Q_{Ao-PA}$  ranged from 1.27 to 3.56 L/min. Most of these patients had large venovenous collaterals exceeding 30% of cardiac output. The exception to this was a single adult patient with a Fontan fenestration and two pediatric patients whose high-output

state was otherwise unexplained. Patients with high shunt fraction (13 of 75) exceeding 30% of cardiac output tended to a high-output state with mean cardiac index of 3.64 L/min/m<sup>2</sup>, as high as 5.82 L/min/m<sup>2</sup>. Exceptions included a few patients with atrioventricular canal or hypoplastic left heart with low-normal cardiac index ranging from 2.13 to 2.96 L/min/m<sup>2</sup>.

In our group of patients who underwent MRI (Table E1 [supplement]), four had systolic ventricular failure requiring transplantation, all of whom were adults. Three exhibited low output failure, with cardiac index near 2.5 L/min/m<sup>2</sup>, and one had high output failure, with cardiac index near 4.0 L/min/m<sup>2</sup>. Four

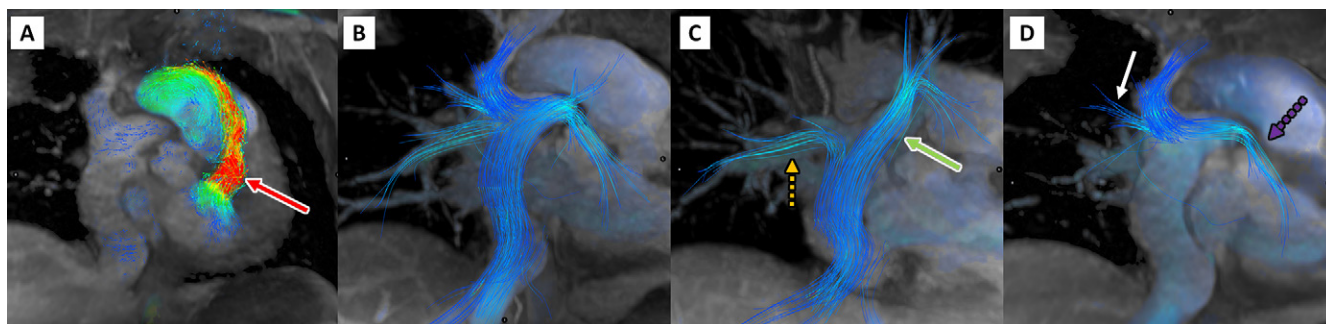


**Figure 5:** Four-dimensional flow visualization of Fontan circuit and caval flow distribution in a 27-year-old man with double-inlet left ventricle and Fontan palliation. In **A**, there is flow acceleration across the bulboventricular foramen. **(B)** Streamlines show distribution of Fontan, or inferior vena cava, flow and Glenn, or superior vena cava, flow to both lungs. **(C)** Fontan, or inferior vena cava, flow streams preferentially into the right lower lobe (orange dashed arrow) and left lung (green arrow), while in **D** Glenn, or superior vena cava, flow streams preferentially into the right upper lobe (white arrow) and left lower lobe (purple dashed arrow).

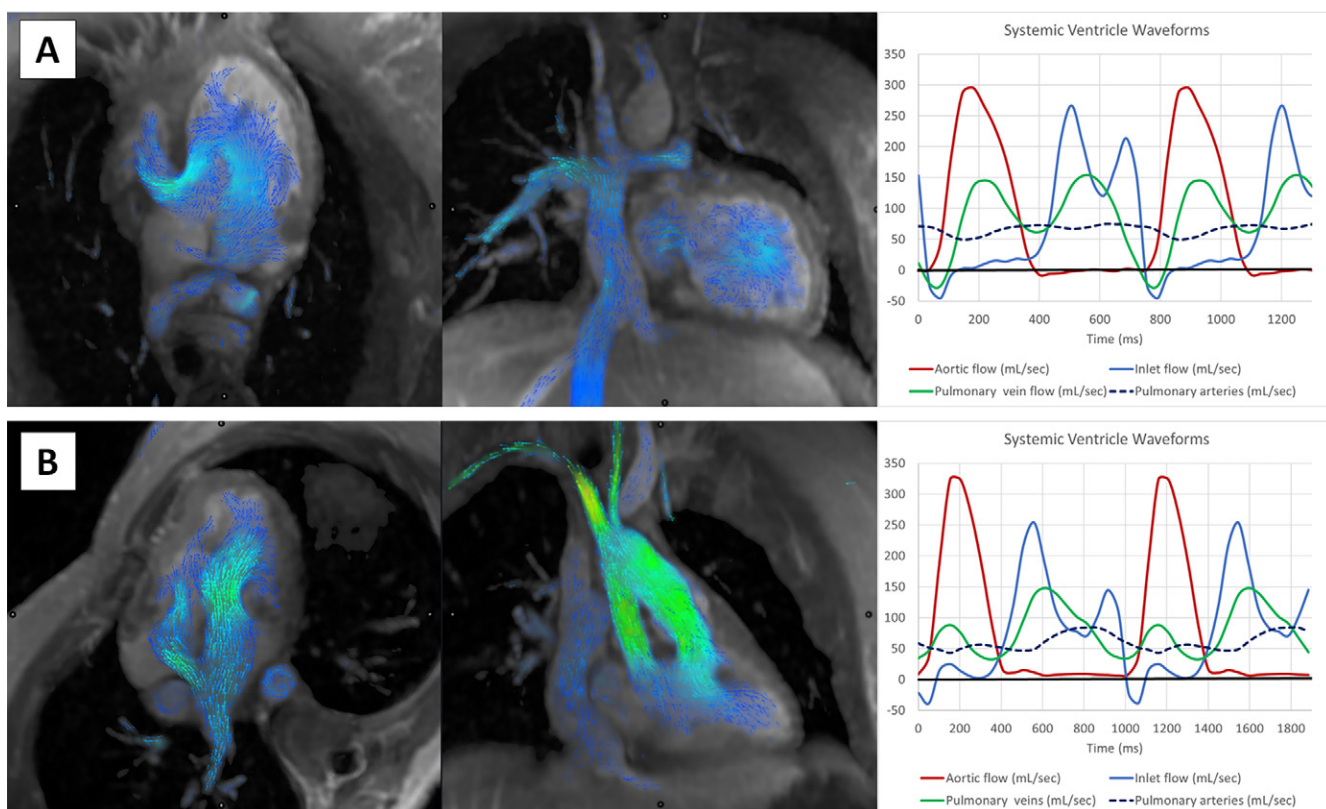


**Figure 6:** Visualization of the Fontan circuit and flow volume waveforms with four-dimensional flow MRI. **(A)** In the top row, images in an 18-year-old woman with tricuspid atresia and Fontan palliation. Mitral inflow volume curves show normal E/A ratio and equal pulmonary venous systolic and diastolic waves. **(B)** In the bottom row, images in a 29-year-old man with double-outlet right ventricle and Fontan palliation with depressed systolic function and moderate diastolic dysfunction. Mitral inflow volumes show normal E/A ratio but depressed pulmonary venous systolic wave and increased pulmonary venous diastolic wave.

patients exhibited moderate or severe atrioventricular valve regurgitation at 4D flow or echocardiography. Four patients developed lymphatic complications, including protein-losing enteropathy or plastic bronchitis. Overall, patients with high output of greater than 4.0 L/min/m<sup>2</sup> tended to be younger (mean age, 11 years; range, 5–27 years), while those with low output of less than 2.5 L/min/m<sup>2</sup> were older (mean age, 26 years; range, 15–34 years).

## Discussion

We illustrate here the feasibility of using 4D flow MRI to assess multiple facets of Fontan physiology and observed an un-

expectedly high frequency of patients in a high-output state across several centers. Though aortopulmonary collaterals are conventionally considered the primary source of shunting in patients with a Fontan circuit, we found relatively few aortopulmonary collaterals in the patients in this study, which are readily identified by tracing their origin from the aorta. Presumably, most aortopulmonary collaterals were ligated earlier in childhood. In contrast to conventional wisdom, we identified venovenous shunting as a principal mode of severe shunting in our patient sample, which was composed of a larger proportion of older patients than in prior studies. We observed a

flow volume step-up in the right pulmonary veins or directly into the atrium, and less frequently in the left pulmonary veins. The severity of venovenous shunting appeared to contribute substantively to high cardiac output state—consequential not only for cyanosis as conventionally thought, but also high-output Fontan failure. Finally, we observed that cardiac output may be an underappreciated benchmark of the health of the Fontan circuit. Routine measurement of cardiac index may complement ventricular volume and ejection fraction, which are more routinely measured.

Previous retrospective surveys of MRI analysis in pediatric patients showed benefit of routine MRI to alter and benefit clinical management (22) and modest correlation of the degree of systemic-to-pulmonary venous collateral flow to ventricular volume loading, central venous pressure, serum brain (or b-type) natriuretic peptide, and poor functional class (23). Perhaps most closely related to the current work is a prior observation that decreased caval return via the Fontan circuit had the strongest correlation to poor clinical condition and age (24). The results of the current study suggest that quantification of cardiac output and severity of shunting should be important benchmarks for assessing the Fontan circuit and may be as important as ejection fraction, which is more universally measured. Cardiac output, while readily measured with phase-contrast MRI, is currently principally obtained at many institutions during invasive catheter angiography or right heart catheterization, though recent data indicate that 4D flow can serve an equivalent noninvasive role (18).

4D flow MRI has recently emerged as a clinically viable technology, benefiting from recent innovations in MRI and scalable cloud-native computation to enable navigation of the geometries of patients with complex congenital heart disease. This has become feasible in the clinical environment due to advances in equipment, pulse sequence design, and advanced postprocessing software (25–27). With this technology, we show it is now possible to carefully interrogate venous blood flow volume at multiple points along the Fontan circuit to precisely pinpoint the nature of collateral shunting. From this experience, we observe that shunt lesions are very common in this population, predominantly through venovenous collaterals that decompress the passive systemic venous return, bypassing directly into the pulmonary venous system and atrium. Our results mirror the experience of catheterization studies of pediatric (28) and adult (4,29) patients with a Fontan circuit in observing a high frequency of these collaterals.

Several caveats should be considered. Quantitative evaluation of 4D flow MRI was not possible in 14 of the original 89 patients due to extensive dephasing artifacts from prior coil embolization and were excluded. Older-generation embolic coils were often made from steel, a ferromagnetic material that causes an exaggerated artifact on MR images, precluding visualization of neighboring vessels. Steel coils have been gradually phased out by newer-generation coils made of titanium alloys such as nitinol (30), which do not produce such artifacts. Nevertheless, we follow many patients who underwent embolization with steel coils at a young age. For such patients, we may perform CT angiography with a delayed venous phase to visualize the collaterals but are left

to speculate their hemodynamic significance on the basis of their size, clinical symptoms, and degree of hypoxia. In addition, at all centers in our study, 4D flow MRI was performed after contrast-enhanced MR angiography. While intravenous contrast agents are not required for the phase-contrast technique, contrast agent administration helps to maximize the signal-to-noise ratio of the velocity measurements. The use of intravenous contrast agents may have mitigated the high  $v_{enc}$  speeds used in some patients at some sites, where in retrospect, lower  $v_{enc}$  of 100–150 cm/sec could have improved visualization and reduced flow measurement error. Finally, the two readers of the study were each highly experienced and capable of measuring flow from complex geometries of the Fontan circulation. Novice users may not achieve high agreement for all vessels, particularly the measurement of the right pulmonary artery, which often has an oblique orientation and is often branched adjacent to the Glenn anastomosis.

Several additional limitations to our study should be considered. Due to the multicenter nature of this study and complex and variable nature of venous shunts, we could not directly compare shunt fraction quantification against degree of cyanosis or invasive catheterization, though the latter was undertaken in prior work (18). Perhaps more importantly for clinical management, because venovenous collaterals may continue to develop in patients with a Fontan circuit without a subpulmonic ventricle, it is unclear which patients should undergo embolization, at what time, and how aggressively this should be pursued and managed. In addition to the cyanosis caused by right-to-left shunting, venovenous collaterals may contribute to excess volume loading of the systemic ventricle, which can be particularly problematic for morphologic right ventricles already straining against the systemic afterload. It remains unclear how much shunting can be tolerated in this patient population, and for each morphologic entity. Earlier investigations have suggested that embolization of venovenous collaterals was associated with decreased survival (31), though it is unclear in this retrospective study whether reduced survival was a consequence of embolization or a consequence of more advanced Fontan failure. Our study suggests that 4D flow may allow us to quantify the hemodynamic impact of venovenous collaterals to guide which ought to be embolized. For the purposes of our study, we applied somewhat arbitrary thresholds of 1.00 L/min for overall shunt volume or 750 mL/min for a given target vessel, roughly 2 standard deviations of interobserver agreement of expert readers in our study, but thresholds required for intervention deserve further investigation. In addition, early investigations have begun to examine the lymphatic abnormalities associated with pediatric Fontan circulation (32), which may also contribute to later Fontan failure. The relationship between venous and lymphatic abnormalities in patients with a Fontan circuit remains unknown.

In addition, we did not fully explore technical considerations for 4D flow in the scope of this work, such as optimal flip angle, acceleration factors, and  $v_{enc}$  speed. It is possible that not all implementations of 4D flow may achieve the precision in flow measurements required to detect small venovenous shunts. In addition, we anecdotally report feasibility of measuring pulmonary venous flow volume waveforms in addition to inlet valve and aortic waveforms in two of our

patients. The feasibility of obtaining these waveforms even in some patients speaks to the quality of the underlying flow volume data. However, we did not fully explore the reliability of these flow waveforms in this study. Thorough investigation of 4D flow technical factors should be considered in future work to further improve the reliability of temporally resolved flow volume waveforms from these slow-flow vessels, and to assess their clinical value relative to echocardiography. We also observed that some flow measurements showed greater interobserver consistency than others. Some paralleled the relative complexity in measurement and frequency of factors known to confound flow measurement, such as complex geometry and nonlaminar flow (33). We expected greater interobserver error for the right pulmonary artery, which can have complex morphology near the Glenn anastomosis. However, interobserver agreement was high at this location, perhaps because of greater attention to this location by the two expert readers.

From the technical point of view, 4D flow MRI has become increasingly available with productization by one of the MRI machine manufacturers and thus is no longer isolated to few academic centers with the research infrastructure previously required to provide this advanced MRI technology. It has previously been shown superior to two-dimensional phase-contrast MRI in consistency of measurement of aortic and pulmonary flow (12), and its quantification of shunt fraction strongly correlates with catheter angiography (18). We share our cumulative experience over several years from three centers where we have adopted 4D flow into our clinical routine. 4D flow MRI acquisition complements the traditional components of our cardiac MRI examinations, enabling more comprehensive evaluation of not only cardiac function and assessment of myocardial tissue, but also hemodynamics, which have long been the purview of echocardiography. We find MRI to be complementary to echocardiographic imaging, able to provide interrogation of structures obscured from sonographic windows, and essential to management of patients with congenital heart disease. The current work highlights the application of 4D flow for assessing the Fontan circuit, complementing prior works, and suggests that this technology should be considered an essential component of a comprehensive congenital heart MRI.

**Author contributions:** Guarantors of integrity of entire study, H.E.S., A.H.; study concepts/study design or data acquisition or data analysis/interpretation, all authors; manuscript drafting or manuscript revision for important intellectual content, all authors; approval of final version of submitted manuscript, all authors; agrees to ensure any questions related to the work are appropriately resolved, all authors; literature research, F.R., D.M., R.C., E.P., H.E.S., A.H.; clinical studies, F.R., D.M., E.P., D.K., N.B., D.B., M.A., H.E.S., A.H.; statistical analysis, D.M., E.P., A.H.; and manuscript editing, F.R., D.M., E.P., D.B., M.A., H.E.S., L.A., A.H.

**Disclosures of conflicts of interest:** F.R. No relevant relationships. D.M. No relevant relationships. R.C. Consultant for Arterys until 2018. E.P. No relevant relationships. D.K. No relevant relationships. N.B. No relevant relationships. D.B. No relevant relationships. M.A. Consulting for GE Medical, not related to this work, no consulting fees received for this article; payment received for presentation given for GE Healthcare and Educational Symposium, not related to this article; payment received for expert witness testimony and consultation, not related to this article; support received for attending meetings, with paid travel by GE Healthcare, Educational Symposia, and Arterys, not related to this article. H.E.S. No relevant relationships. L.A. No relevant relationships. A.H. Research grant support from GE Healthcare and Bayer; royalties or licenses from Stanford University; patent issued

to Stanford University for comprehensive cardiovascular analysis with volumetric phase-contrast MRI; stock/stock options as co-founder of Arterys.

## References

- Diller GP, Giardini A, Dimopoulos K, et al. Predictors of morbidity and mortality in contemporary Fontan patients: results from a multicenter study including cardiopulmonary exercise testing in 321 patients. *Eur Heart J* 2010;31(24):3073–3083.
- Fontan F, Baudet E. Surgical repair of tricuspid atresia. *Thorax* 1971;26(3):240–248.
- d'Udekem Y, Iyengar AJ, Galati JC, et al. Redefining expectations of long-term survival after the Fontan procedure: twenty-five years of follow-up from the entire population of Australia and New Zealand. *Circulation* 2014;130(11 Suppl 1):S32–S38.
- Rychik J, Atz AM, Celermajor DS, et al. Evaluation and Management of the Child and Adult with Fontan Circulation: A Scientific Statement from the American Heart Association. *Circulation* 2019;140(6):e234–e284.
- Ginde S, Goot BH, Frommelt PC. Imaging adult patients with Fontan circulation. *Curr Opin Cardiol* 2017;32(5):521–528.
- Rathod RH, Prakash A, Powell AJ, Geva T. Myocardial fibrosis identified by cardiac magnetic resonance late gadolinium enhancement is associated with adverse ventricular mechanics and ventricular tachycardia late after Fontan operation. *J Am Coll Cardiol* 2010;55(16):1721–1728.
- Grosse-Wortmann L, Al-Otay A, Yoo S-J. Aortopulmonary collaterals after bidirectional cavopulmonary connection or Fontan completion: quantification with MRI. *Circ Cardiovasc Imaging* 2009;2(3):219–225.
- Ghelani SJ, Harrild DM, Gauvreau K, Geva T, Rathod RH. Comparison Between Echocardiography and Cardiac Magnetic Resonance Imaging in Predicting Transplant-Free Survival After the Fontan Operation. *Am J Cardiol* 2015;116(7):1132–1138.
- Whitehead KK, Gillespie MJ, Harris MA, Fogel MA, Rome JJ. Noninvasive quantification of systemic-to-pulmonary collateral flow: a major source of inefficiency in patients with superior cavopulmonary connections. *Circ Cardiovasc Imaging* 2009;2(5):405–411.
- Markl M, Geiger J, Kilner PJ, et al. Time-resolved three-dimensional magnetic resonance velocity mapping of cardiovascular flow paths in volunteers and patients with Fontan circulation. *Eur J Cardiothorac Surg* 2011;39(2):206–212.
- Bächler P, Valverde I, Pinochet N, et al. Caval blood flow distribution in patients with Fontan circulation: quantification by using particle traces from 4D flow MR imaging. *Radiology* 2013;267(1):67–75.
- Hsiao A, Alley MT, Massaband P, Herfkens RJ, Chan FP, Vasanawala SS. Improved cardiovascular flow quantification with time-resolved volumetric phase-contrast MRI. *Pediatr Radiol* 2011;41(6):711–720.
- Isorni M-A, Moisson L, Moussa NB, et al. 4D flow cardiac magnetic resonance in children and adults with congenital heart disease: Clinical experience in a high volume center. *Int J Cardiol* 2020;320:168–177.
- Isorni MA, Martins D, Ben Moussa N, et al. 4D flow MRI versus conventional 2D for measuring pulmonary flow after Tetralogy of Fallot repair. *Int J Cardiol* 2020;300:132–136.
- Valverde I, Nordmeyer S, Uribe S, et al. Systemic-to-pulmonary collateral flow in patients with palliated univentricular heart physiology: measurement using cardiovascular magnetic resonance 4D velocity acquisition. *J Cardiovasc Magn Reson* 2012;14(1):25.
- Feneis JF, Kyubwa E, Atianzar K, et al. 4D flow MRI quantification of mitral and tricuspid regurgitation: Reproducibility and consistency relative to conventional MRI. *J Magn Reson Imaging* 2018;48(4):1147–1158.
- Jacobs K, Rigdon J, Chan F, et al. Direct measurement of atrioventricular valve regurgitant jets using 4D flow cardiovascular magnetic resonance is accurate and reliable for children with congenital heart disease: a retrospective cohort study. *J Cardiovasc Magn Reson* 2020;22(1):33.
- Horowitz MJ, Kupsky DF, El-Said HG, Alshawabkeh L, Kligerman SJ, Hsiao A. 4D Flow MRI Quantification of Congenital Shunts: Comparison to Invasive Catheterization. *Radiol Cardiothorac Imaging* 2021;3(2):e200446.
- Cheng JY, Zhang T, Ruangwattanapaisarn N, et al. Free-breathing pediatric MRI with nonrigid motion correction and acceleration. *J Magn Reson Imaging* 2015;42(2):407–420.
- Winkelmann S, Schaeffter T, Koehler T, Eggers H, Doessel O. An optimal radial profile order based on the Golden Ratio for time-resolved MRI. *IEEE Trans Med Imaging* 2007;26(1):68–76.
- Cheng JY, Alley MT, Cunningham CH, Vasanawala SS, Pauly JM, Lustig M. Nonrigid motion correction in 3D using autofocusing with localized linear translations. *Magn Reson Med* 2012;68(6):1785–1797.
- Zaki NC, Kelleman MS, James Parks W, Slesnick TC, McConnell ME, Oster ME. The utility of cardiac magnetic resonance imaging in post-Fontan surveillance?. *Congenit Heart Dis* 2019;14(2):140–146.

23. Kodama Y, Ishikawa Y, Kuraoka A, et al. Systemic-to-Pulmonary Collateral Flow Correlates with Clinical Condition Late After the Fontan Procedure. *Pediatr Cardiol* 2020;41(8):1800–1806.
24. Ovroutski S, Nordmeyer S, Miera O, et al. Caval flow reflects Fontan hemodynamics: quantification by magnetic resonance imaging. *Clin Res Cardiol* 2012;101(2):133–138.
25. Zhong L, Schrauben EM, Garcia J, et al. Intracardiac 4D Flow MRI in Congenital Heart Disease: Recommendations on Behalf of the ISMRM Flow & Motion Study Group. *J Magn Reson Imaging* 2019;50(3):677–681.
26. Cheng JY, Hanneman K, Zhang T, et al. Comprehensive motion-compensated highly accelerated 4D flow MRI with ferumoxytol enhancement for pediatric congenital heart disease. *J Magn Reson Imaging* 2016;43(6):1355–1368.
27. Hsiao A, Lustig M, Alley MT, Murphy MJ, Vasanaawala SS. Evaluation of valvular insufficiency and shunts with parallel-imaging compressed-sensing 4D phase-contrast MR imaging with stereoscopic 3D velocity-fusion volume-rendered visualization. *Radiology* 2012;265(1):87–95.
28. Heinemann M, Breuer J, Steger V, Steil E, Sieverding L, Ziemer G. Incidence and impact of systemic venous collateral development after Glenn and Fontan procedures. *Thorac Cardiovasc Surg* 2001;49(3):172–178.
29. Evans WN, Acherman RJ, Mayman GA, et al. Fontan venovenous collaterals and hepatic fibrosis. *J Card Surg* 2020;35(11):2974–2978.
30. Florian G, Gabor AR, Nicolae CA, et al. Thermomechanical, calorimetric and magnetic properties of a Ni–Ti shape-memory alloy wire. *J Therm Anal Calorim* 2020;140(2):527–544.
31. Poterucha JT, Johnson JN, Taggart NW, et al. Embolization of Venovenous Collaterals after the Fontan Operation Is Associated with Decreased Survival. *Congenit Heart Dis* 2015;10(5):E230–E236.
32. Biko DM, DeWitt AG, Pinto EM, et al. MRI evaluation of lymphatic abnormalities in the neck and thorax after Fontan surgery: Relationship with outcome. *Radiology* 2019;291(3):774–780.
33. Contijoch FJ, Horowitz M, Masutani E, Kligerman S, Hsiao A. 4D Flow Vorticity Visualization Predicts Regions of Quantitative Flow Inconsistency for Optimal Blood Flow Measurement. *Radiol Cardiothorac Imaging* 2020;2(1):e190054.